

# A Non-Linear Model for the Rapid Prediction of the Magnetic Field in Eccentric Synchronous Reluctance Machines

Hossein Hooshmandi Safa, Hossein Abootorabi Zarchi

**Abstract**— This paper introduces a novel numerical model for the fast characterization of concentric and eccentric synchronous reluctance motors (SynRMs) used in electric vehicles (EVs) applications. Regarding the high impact of the air gap and permeance function on the modeling accuracy, a step variation function is used to consider the flux barriers effect on the air gap. Then different types of eccentricity including, static, dynamic, and mixed eccentricity are modeled. Besides, this model considers the magnetic saturation and the stator slots effect. Numerical computation for the motor inductances is applied to avoid any approximation in the permeance function. The air gap flux density, electromagnetic torque, and the radial force on the rotor are then calculated. This model can be used for the preliminary design of SynRMs to analyze motor performance in different conditions and accelerate design procedure. The model is simply adjustable to different configurations. For instance, a 4-pole single layer distributed winding machine with 36-slot, and 3-flux barriers per pole is investigated. In order to verify the proposed model, the obtained results are compared with finite element analysis (FEA) and experimental tests. The accuracy of the proposed model for eccentricities up to 30 percent is 98%, and for higher degrees, is about 95%.

**Index Terms**— Electric vehicles, Synchronous reluctance machines, Eccentricity, Flux density, Finite element method

## I. INTRODUCTION

The electric motors are one of the most important parts of electric vehicles (EVs). Regarding high torque and speed, wide speed range, and high efficiency, the synchronous reluctance motors (SynRMs) possesses a good potential for the EVs application [1]. In recent years, lots of research has been done to improve SynRM's performance for use in EVs [2-5]. The SynRMs rely on the magnetic reluctance principle to produce torque. They use a traditional stator concept similar to the industrial induction motors. The rotor is made of steel lamination only, with the distributed flux barriers. In order to improve safety and reduce repairing costs, electrical motors should be protected versus different faults. There are three types of eccentricity that include static eccentricity (SE), dynamic eccentricity (DE), and mixed eccentricity (ME). In SE, the rotor axis and the rotation axis are the same, but they are shifted from the stator axis. In DE, the stator axis and the rotation axis are the same, while the rotor is displaced from the stator axis. In ME, unlike SE, the minimum air gap is dependent on the rotor position.

Hossein Hooshmandi Safa and Hossein Abootorabi Zarchi are with Department of Engineering, Ferdowsi University of Mashhad.  
(Email: hossein.hooshmandi@mail.um.ac.ir; abootorabi@um.ac.ir.)

In ME, the rotor, stator, and rotation axis are different from each other, and the air gap varies with the rotor rotation [6].

There are some degrees of eccentricity in the practical electrical machines due to the production inaccuracy and bearing tolerance. Eccentricity produces an electromagnetic force, also named as unbalanced magnetic pull (UMP) that interacts between the rotor and stator. The UMP inclines to intensify the eccentricity, and may cause abrasion of the rotor and stator. Furthermore, the UMP caused by the eccentricity results in increasing vehicle vibration and reducing riding security. Therefore, eccentricity analysis should be fulfilled in the design process of the electric machines, especially in EVs application for electrical and mechanical considerations. For this purpose, a fast and accurate method is needed to calculate the magnetic flux density in the eccentric motor.

In [7,8], a conformal mapping and the magnetic equivalent circuit (MEC) have been used to calculate the reluctance of the rotor flux barriers in the concentric SynRMs. The result then has been employed to analytically determine the distribution of the air gap flux density and the electromagnetic torque. In [9], an analytical method has been proposed for the characterization of the concentric SynRMs. In [10,11], the conformal mapping method has been used for the UMP analysis in the permanent magnet machines. An analytical model for the UMP calculation in the eccentric induction motor considering the cage rotor's damping effect has been presented in [12]. In [13], a method for dynamic simulation of the induction motors, including mixed eccentricity and UMP, has been introduced. The magnetizing current, which is calculated by FEM, is used for the simplification of the UMP model. In [14], the UMP and the induced electromotive forces have been studied for the eccentric round rotor synchronous machine. In [15], a mathematical model for analyzing the eccentricity effect on the UMP in the large vertical shaft synchronous machines has been presented.

Although, the UMP caused by the eccentricity in the induction motors [16-20], PMSMs [21-25], and salient pole synchronous machines [14-15], are comprehensively investigated, there are a few publications on the SynRMs with eccentricity. In [26], an analytical method based on the (MEC) has been proposed to predict the performance of the eccentric synchronous reluctance motor. However, due to approximation in the air gap definition, it is not suitable for the eccentricity fault modeling and diagnosis. For the comparison, a simplified finite element model (FEM) without considering the stator slots and saturation effects has been used. In [27-28], the magnetic potential, the magnetic field density, and torque have been

computed using MEC for the concentric and eccentric SynRMs, respectively. However, the models like this, which used the current supply as an input, are not appropriate for the fault diagnosis purposes such as motor current signature analysis (MCSA).

According to the abovementioned review, there is still no rapid and accurate approach to consider eccentricity for the dynamic simulation of SynRMs with flux barriers. This paper aims to fill this void by presenting a novel approach for the accurate calculation of the air gap permeance function considering the rotor flux barriers, eccentricity, saturation, and the stator slots effect. For the first time, the modified winding function method (MWFM) is employed to model the eccentric SynRMs using the calculated air gap permeance. The calculation of the motor inductances are fulfilled by numerical procedure, which does not require any approximation for the turn function, modified winding function, and the air gap function. The two-dimensional time-stepping finite element method and the experimental tests are exploited to verify the proposed model results. The other contributions of this paper are listed as follows:

- This model can be used for the preliminary design of the SynRMs to analyze the motor performance and accelerate the design procedure. The introduced model is significantly faster than the FEM. The simulation time in the presented model is a few seconds, while the FEM takes several hours. Moreover, there is good agreement between the proposed model results and the FEM. The computed radial force under the eccentricity condition can be used for the mechanical design of the rotor in the high-speed region to design fault tolerable motor and improve motor safety.
- In addition to being used in the motor design process, the proposed method provides a fast simulation tool for analyzing the motor signals like the current and torque in the time or frequency domain to extract the proper indices for the eccentricity fault diagnosis in the SynRMs. The extracted index can be used in the real-time drive system to detect the eccentricity at incipient level.

This paper is organized as follows: In section II, the dynamic model of SynRMs is brought. Section III presents the air gap modeling. The inductance calculation is discussed in section IV. In section V the flux density, torque, and force computation are presented. The simulation of the model is discussed in section VI. Section VII introduces motor modeling using the FEM. Section VIII describes the experimental set-up. The simulation and experimental results are discussed in section IX. Finally, the conclusion is remarked in section X.

## II. DYNAMIC MODEL OF SYNRM

The multiple coupled circuit approach is used to express the voltage and current relationship. A three-phase sinusoidal voltage is used to stimulate stator windings. Voltages across the stator windings are defined by:

$$\begin{bmatrix} v_a \\ v_b \\ v_c \end{bmatrix} = \begin{bmatrix} R_s & 0 & 0 \\ 0 & R_s & 0 \\ 0 & 0 & R_s \end{bmatrix} \begin{bmatrix} i_a \\ i_b \\ i_c \end{bmatrix} + \begin{bmatrix} \frac{d\psi_a}{dt} \\ \frac{d\psi_b}{dt} \\ \frac{d\psi_c}{dt} \end{bmatrix} \quad (1)$$

Where  $v$  is the individual phase voltage,  $R_s$  is the equivalent resistance of each stator winding,  $i$  is the phase current,  $\psi$  is the flux linking each stator winding, which is defined by:

$$\begin{bmatrix} \psi_a \\ \psi_b \\ \psi_c \end{bmatrix} = \begin{bmatrix} L_{aa} & L_{ab} & L_{ac} \\ L_{ba} & L_{bb} & L_{bc} \\ L_{ca} & L_{cb} & L_{cc} \end{bmatrix} \begin{bmatrix} i_a \\ i_b \\ i_c \end{bmatrix} \quad (2)$$

The electromagnetic torque of the motor at any rotor angle is calculated based on the co-energy method and using the winding inductances as follows

$$T_e = \frac{1}{2} [I]^T \left[ \frac{\partial L(\theta_r)}{\partial \theta_r} \right] [I] \quad (3)$$

$[I]$  is the stator current matrix, and  $L$  is the stator inductance matrix. The electro-mechanical equation of the motor is:

$$T_e - T_L = J \frac{d\omega_r}{dt} + F \omega_r \quad (4)$$

where  $T_e, T_L, j$ , and  $F$  are the electromagnetic and load torque, the inertia moment of the rotor, and the mechanical damping coefficient, respectively. The angular velocity of the rotor is shown as:

$$\omega_r = \frac{d\theta_r}{dt} \quad (5)$$

Based on the equations mentioned above, the stator inductance calculation is needed for solving the dynamic simulation of the SynRMs. For this purpose, the air gap function must first be modeled.

## III. AIR GAP MODELING

For analyzing the machine performance in the eccentricity condition, accurate modeling of the air gap is needed. The mechanical air gap of a healthy SynRMs is uniform. However, the flux barriers form variable magnetic reluctance, which can be considered a secondary effect on the air gap length. In this paper, firstly, the effects of flux barriers, saturation, and slots on the air gap function are modeled. Then the air gap function will be improved to consider the different eccentricities.

Fig. 1 (a) illustrates the rotor cross-section of the SynRM. Fig. 1 (b) demonstrates the individual air gap lengths for each of the flux barriers that lead to the same amount of air gap flux drop. Fig. 1 (c) shows the calculated air gap function using the circular flux barriers. The mechanical air gap length is added to the overall air gap length achieved from the flux barriers. The significance of this model is that it considers the main physical appearance of the flux barriers, and it is easily usable in the MWFM. It should be noted that the proposed method could be used for the characterization of transversally laminated anisotropic SynRMs. Stator slots effect on the air gap can be considered as follows:

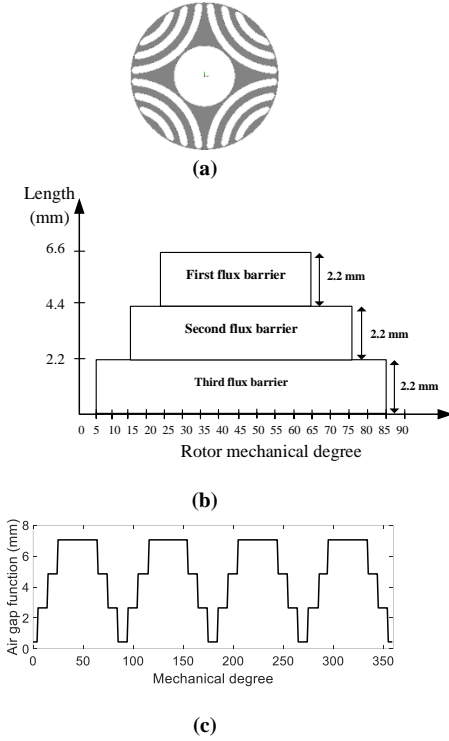


Fig. 1 (a) the rotor cross-section of the SynRM (b) the air gap length of each flux barriers (c) the effective air gap function of the SynRM

$$g(\varphi, \theta_r) = g_{rel} - \delta_{slot} \cos(N_s \varphi) \quad (6)$$

where  $g_{rel}$ ,  $\delta_{slot}$ ,  $N_s$ ,  $\varphi$  and  $\theta_r$  are the effective air gap length related to flux barriers, constant-coefficient related to saturation effect, number of stator slots, angular position in the stator reference frame, and rotor angular position, respectively. For precise modeling of the air gap function, the saturation effect should be estimated. The saturation decreases the magnetic permeability of the iron paths, which increases the reluctance of the area around the saturation. In [29], it has been shown that the air gap length can be used instead of a reduction in the iron permeability to model the saturation in the iron parts. Therefore, the air gap length is defined as a function of the saturation level. Therefore, the air gap function can be represented as:

$$g(\varphi, \theta_r) = g_{rel}(\varphi, \theta_r) - \delta_{slot} \cos(N_s \varphi) - \delta_{sat} \cos(2\omega_s t - P\varphi) \quad (7)$$

where  $\delta_{sat}$ ,  $\omega_s$ , and  $P$  are the constant-coefficient related to saturation effects, angular supply frequency, and the number of pole pairs, respectively.  $\delta_{sat}$  is expressed as follows [29]

$$\delta_{sat} = \frac{2g_0(k_{sat} - 1)}{3k_{sat}} \quad (8)$$

$k_{sat}$  is the saturation factor, which is the ratio of the fundamental components of the air gap voltage for non-saturated and saturated conditions, and  $g_0$  is the mechanical air gap length. In the ME fault, both the SE and DE simultaneously occur. The air gap function in the ME case can be derived as follows

$$g(\varphi, \theta_r) = g_{rel}(\varphi, \theta_r) - \delta_{slot} \cos(N_s \varphi) - \delta_{sat} \cos(2\omega_s t - P\varphi) - \delta_{se} \cos(\varphi) - \delta_{de} \cos(\omega_r t - \varphi) \quad (9)$$

where  $\delta_{se}$  and  $\delta_{de}$  are the SE and DE degrees and represented by (10) and (11), respectively.

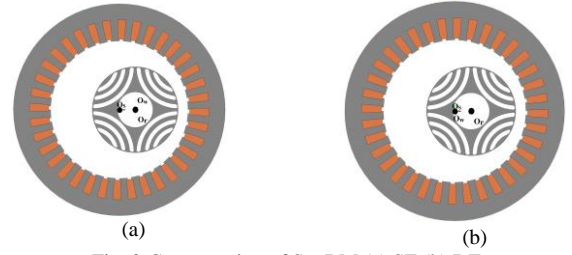


Fig. 2 Cross-section of SynRM (a) SE (b) DE

$$\delta_{se} = \frac{O_s O_w}{g_0} \quad (10)$$

$$\delta_{de} = \frac{O_w O_r}{g_0} \quad (11)$$

where  $O_s$ ,  $O_r$ , and  $O_w$  are the axes of the stator, rotor, and the rotation axes, respectively. Fig. 2 shows the relative position of the stator and the rotor for different eccentricity types.

#### IV. INDUCTANCE CALCULATION OF SYNRM

The winding function method (WFM) is based on the coupled electromagnetic equations, which are achieved using the simple laws of electric circuit theory [30]. All the space harmonics of the machine are taken into account in this approach. In the WFM, it is supposed that the air gap has a uniform distribution. In this case, the winding function is defined as [30]:

$$N(\varphi) = n(\varphi) - \langle n(\varphi) \rangle \quad (12)$$

where  $n(\varphi)$  is the stator turn function, which indicates the winding distribution, and  $\langle n(\varphi) \rangle$  is the average of the turn function shown as:

$$\langle n(\varphi) \rangle = \frac{1}{2\pi} \int_0^{2\pi} n(\varphi) d\varphi \quad (13)$$

The inductance value of phase A due to the current flowing in phase B is calculated as:

$$L_{AB}(\theta_r) = \frac{\mu_0 r l}{g_0} \int_0^{2\pi} n_A(\varphi) N_B(\varphi, \theta_r) d\varphi \quad (14)$$

where  $\mu$ ,  $r$ , and  $l$  are the magnetic permeability of air, rotor outer radius, and the stack length, respectively. Since the air gap variation is not taken into consideration in the inductance calculation, WFM cannot model salient pole or eccentric machines. Therefore, in this paper, for the first time, MWFM is used to model concentric and eccentric SynRMs with distributed flux barriers.

In [31], the WFM has been modified to consider air gap eccentricity. The MWFM of a coil can be expressed as:

$$M(\varphi, \theta_r) = n(\varphi) - \langle M(\theta_r) \rangle \quad (15)$$

where  $n(\varphi)$  is the stator turn function and  $\langle M(\theta_r) \rangle$  is the average of the modified winding function shown as:

$$\langle M(\theta_r) \rangle = \frac{1}{2\pi \langle g^{-1}(\varphi, \theta_r) \rangle} \int_0^{2\pi} n(\varphi) g^{-1}(\varphi, \theta_r) d\varphi \quad (16)$$

where  $\langle g^{-1} \rangle$  is the average of the inverse air gap defined as:

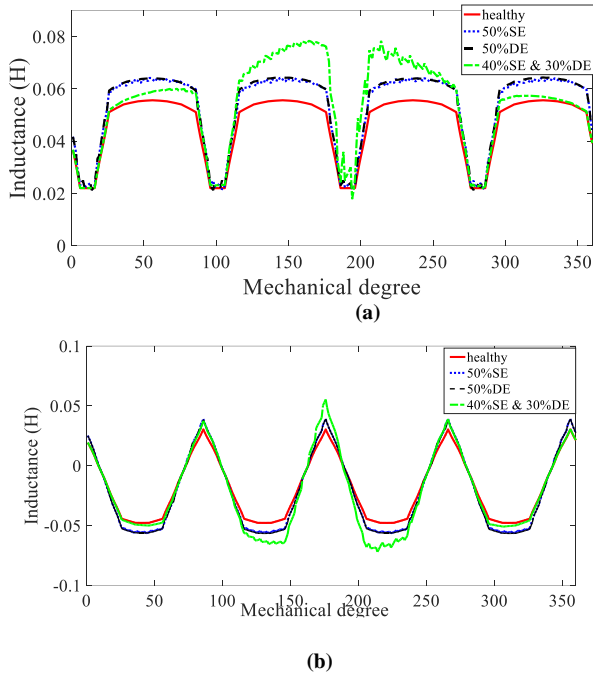


Fig. 3 Stator inductance in healthy and different eccentricity case (a) self inductance of phase a (b) Mutual inductance between phases a and b

$$\langle g^{-1}(\varphi, \theta_r) \rangle = \frac{1}{2\pi} \int_0^{2\pi} g^{-1}(\varphi, \theta_r) d\varphi \quad (17)$$

The inductance value of phase A due to the current flowing in phase B is represented as:

$$L_{AB}(\theta_r) = \mu_0 r \ell \int_0^{2\pi} n_A(\varphi) M_B(\varphi, \theta_r) g^{-1}(\varphi, \theta_r) d\varphi \quad (18)$$

According to the (18), the self and mutual inductances of the machine are dependent on the air gap permeance function ( $g^{-1}$ ). Because of the reluctance nature of the SynRMs, as shown in Fig. 1(c), and regarding the air gap definition in the healthy and eccentricity conditions (7 and 9), the air gap function varies and results in permeance function variation. Therefore, self and mutual inductances profile change with type and degree of eccentricity. Fig. 3 (a) and Fig. 3(b) illustrate the self and mutual inductance of the stator for the healthy motor and motor under different eccentricities, respectively. It can be seen that the values of the inductances are changed regarding the type and degree of the eccentricity. Moreover, the ME makes more distortion in the inductance profile.

## V. FLUX DENSITY, TORQUE, AND FORCE CALCULATION

The proposed model can also calculate the dynamic torque of the SynRMs. The Maxwell Stress Tensor defined in (19) is exploited to predict the electromagnetic torque waveform of the cylindrical coordinate system [32]:

$$\mathbb{T} = \frac{1}{\mu_0} \begin{bmatrix} \frac{B_r^2 - B_\theta^2 - B_z^2}{2} & B_r B_\theta & B_r B_z \\ B_\theta B_r & \frac{B_\theta^2 - B_r^2 - B_z^2}{2} & B_\theta B_z \\ B_z B_r & B_z B_\theta & \frac{B_z^2 - B_r^2 - B_\theta^2}{2} \end{bmatrix} \quad (19)$$

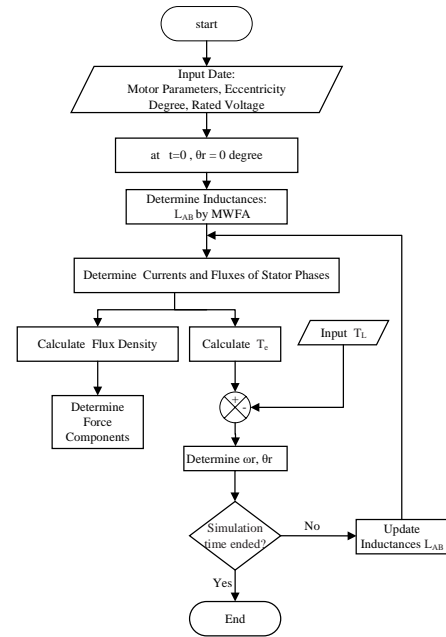


Fig. 4 Flowchart for simulation in MATLAB

where  $B_r$ ,  $B_\theta$ , and  $B_z$  are the radial, tangential, and the  $z$  component of the magnetic flux. The electromagnetic force is defined as

$$\vec{F} = \oint_S \mathbb{T} \cdot \vec{n} ds \quad (20)$$

where  $S$  is a surface enclosing the considered body, and  $\vec{n}$  is a unit vector normal to the surface  $S$ . The radial force on the rotor is calculated as

$$F_r = \int_0^{2\pi} \frac{B_g^2(\varphi) D \ell}{4\mu_0} e^{j\varphi} d\varphi \quad (21)$$

The  $F_x$  and  $F_y$  components of radial force can be computed as [26]:

$$F_x = \int_0^{2\pi} \frac{B_g^2(\varphi) D \ell}{4\mu_0} \cos(\varphi) d\varphi$$

$$F_y = \int_0^{2\pi} \frac{B_g^2(\varphi) D \ell}{4\mu_0} \sin(\varphi) d\varphi \quad (22)$$

where  $B_g$  is the air gap flux density, and  $D$  is the inner diameter of the stator. The flux density in the air gap produced by the  $i$ th winding is expressed as [33]:

$$B_i(\varphi, \theta_r) = \mu_0 \frac{M_i(\varphi, \theta_r)}{g(\varphi, \theta_r)} i_i \quad (23)$$

where  $i_i$  is the current flowing through the  $i$ th winding.

## VI. SIMULATION OF THE PROPOSED MODEL

The simulation of the proposed model is carried out for a time duration of 12 s with a time step of (1/2048) s in MATLAB using the Intel Core i7 processor, 2.6 GHz, 16GB RAM computer. Therefore, the total number of iterations is 24576. The simulation of the proposed method takes 9.54 s to complete. The flowchart of the proposed model for simulation in MATLAB is depicted in Fig. 4. The motor parameters are presented in Table I.



Table I : Motor parameters

Rated power	350 W
Rated speed	1500 rpm
Stator pole pairs number	2
Number of stator slots	36
Flux barriers number per pole	3
Air gap	0.45 mm
rotor outer diameter	94 mm
Stack length	50 mm

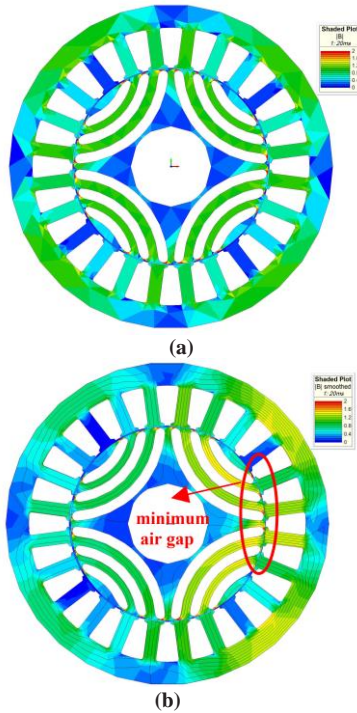


Fig. 5 flux density distribution of the (a) healthy motor (b) motor with 50%SE

## VII. MOTOR MODELING USING FEM

Infolytica MagNet software is used for 2D finite element modeling of the motor. In this model, the physical complexities of all parts of the motor and the non-linear property of the materials are taken into account. A transient with motion solver is used for the simulation. Fig. 5 shows the flux density distribution of the healthy motor and the motor with 50%SE. As can be seen, the SE increases the flux density in the region that the air gap has a minimum length (right-hand side of the motor). The torque on the rotor, motor flux density, and the  $x$ - $y$  component of the radial force obtained from the FEM simulation has been discussed in section IX and compared with the proposed model.

## VIII. EXPERIMENTAL SETUP

The test bench is illustrated in Fig. 6. The voltage source inverter is used in the setup. A Texas Instrument signal processor TMS320F28335 and Hall-effect current and voltage

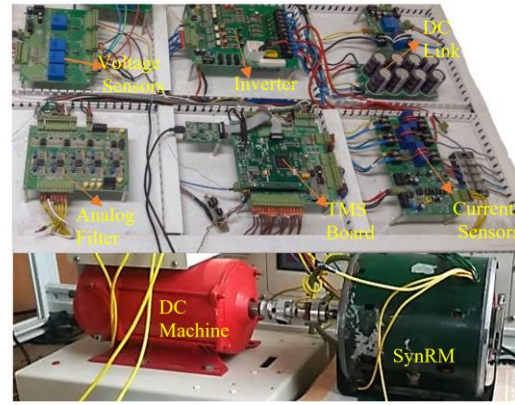


Fig. 6 Experimental setup

sensors are used for the control system. Moreover, to filter current and voltage signals, an analog second-order low pass filter is exploited. Torque is measuring by transferring force to the high-sensitive load-cells. A DC generator and a rheostat are used to adjust the output power. Various methods used in the literature to create different types of eccentricity have been reviewed in [34]. In this paper, to create eccentricity in the motor, the main bearing is replaced with another bearing with a larger inner diameter and smaller outer diameter. In order to induce the static eccentricity, a concentric inner ring and an eccentric outer ring are used between the rotor shaft and the bearing as well as between the bearing and the housing, respectively. Moreover, to create dynamic eccentricity, an eccentric inner ring is used between the rotor shaft and the bearing; also, a concentric outer ring is used between the bearing and the housing. In the case of mixed eccentricity, both the inner and outer rings are eccentric. The value of eccentricity can be determined accurately by the machining of the inner and outer rings.

## IX. RESULTS AND DISCUSSIONS

All simulation and experimental test are carried out at the rated speed and rated load. Fig. 7 depicts the phase current waveforms in 50 %SE obtained from the proposed model. Fig. 8 (a) shows the distribution of the radial component of the flux density in the air gap resulting from the proposed model, which is compared with the FEM for the healthy motor. For comparison, the introduced model in [26], which is based on the MEC, is depicted in Fig.8 (a). It is evident that the flux density obtained through the MEC is far from the real flux density distribution. Fig. 8 (b) displays the distribution of the tangential component of the flux density in the air gap resulting from the proposed model compared with the FEM for the healthy motor.

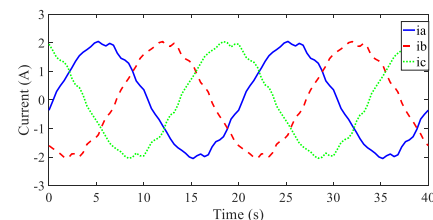


Fig. 7 Phase current waveforms in 50%SE

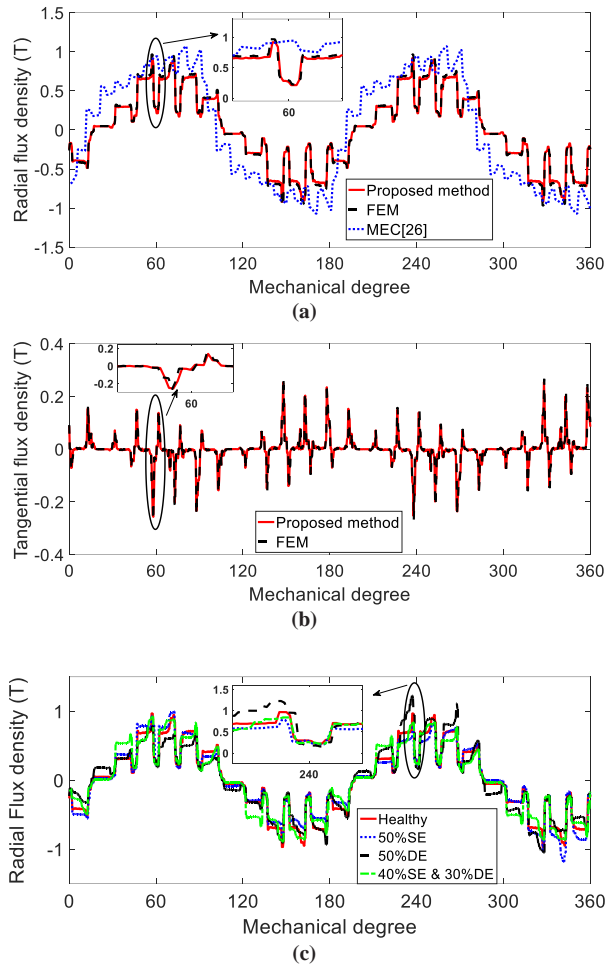


Fig. 8 Air-gap flux density distribution resulting from the proposed method and FEM (a) radial component for healthy motor (b) tangential component for healthy motor (c) radial component resulting from the proposed method for healthy motor and motor with different eccentricities

It can be seen that there is a good agreement between the results of the proposed model in this paper and the FEM results. Moreover, Fig. 8 (c) illustrates the comparison of the radial components of the air gap flux density for the healthy motor and the motor with different eccentricities. By comparing the different cases in Fig. 8(c), it can be understood that the eccentricity causes the asymmetrical distribution in the air gap flux density, which distorts the stator current and torque of the motor.

As shown in section V, the  $x - y$  components of the radial force acting on the rotor can be predicted in the different healthy and faulty cases using the equation (21). Fig. 9 depicts the radial force components  $F_x$  and  $F_y$  resulting from the presented model and FEM for the healthy motor and motor with different eccentricities. Fig. 9 (a) demonstrates the radial force components  $F_x$  and  $F_y$  in the healthy motor. The radial force components are almost zero in this case. Fig. 9 (b) shows  $F_y$

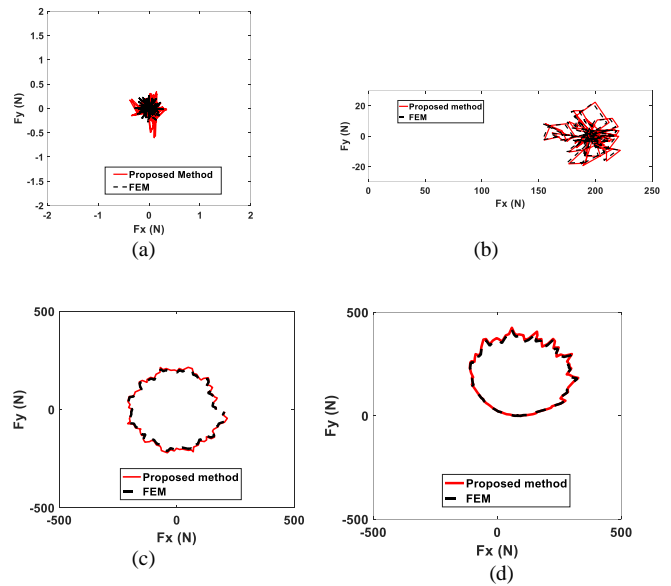


Fig. 9  $F_y$  versus  $F_x$  acting on the rotor of the SynRM at all rotor position resulting from both the proposed method and FEM (a) healthy motor (b) motor with 20% SE (c) motor with 20% DE (d) motor with 10% SE and 20% DE

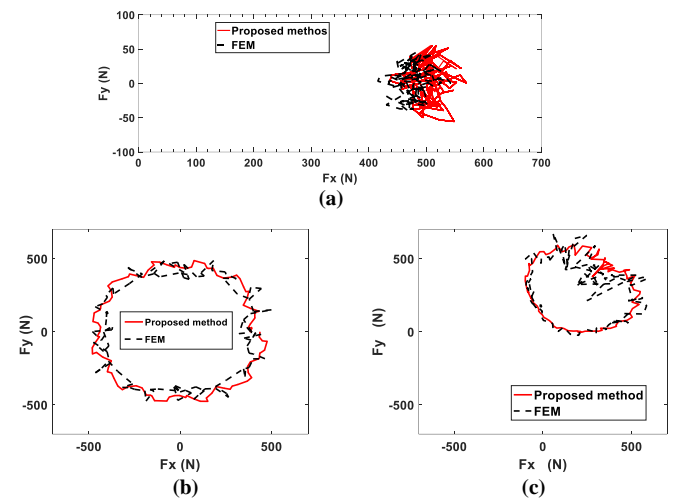


Fig. 10  $F_y$  versus  $F_x$  acting on the rotor of the SynRM at all rotor position resulting from both the proposed method and FEM (a) motor with 50% SE (b) motor with 50% DE (c) motor with 40% SE and 30% DE

versus  $F_x$  in 20%SE. The force is in the direction of the minimum air gap. The FEM and proposed model predict a force in the range between 220 and 222 N, respectively. In 20%DE, as shown in Fig. 9 (c), due to rotating the minimum air gap length, the radial force revolves with the rotor. In this case, the radial force is 216 and 220 N for the FEM and proposed models, respectively. Fig. 9 (d) illustrates the radial force components for the ME case with 10%SE and 20%DE. In this case, the radial force is 417 and 425 N for the FEM and proposed model, respectively. The comparison between the results of the proposed model and FEM indicates that there is an excellent compromise in different eccentricity types.

Table II :Peak value of the radial force on the rotor

Eccentricity Type	Static eccentricity %		Dynamic eccentricity %		Mixed eccentricity %		
	Eccentricity degree	20%SE	50%SE	20%DE	50%DE	10%SE & 20%DE	40%SE & 30%DE
The proposed model results (N)		222	570	220	475	425	550
The FEM results (N)		220	545	216	500	417	570

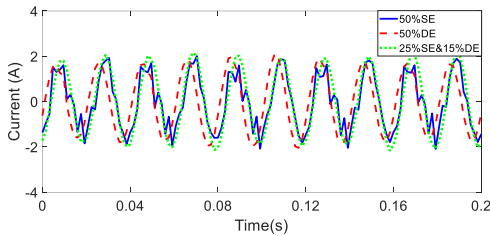


Fig. 11 Current waveform in different eccentricity cases (experiment)

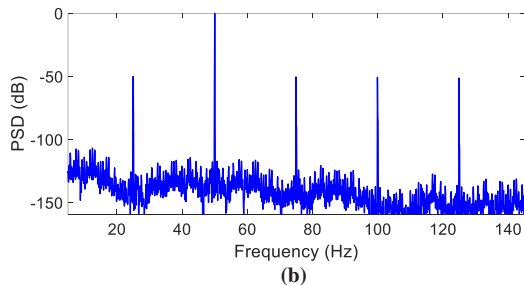
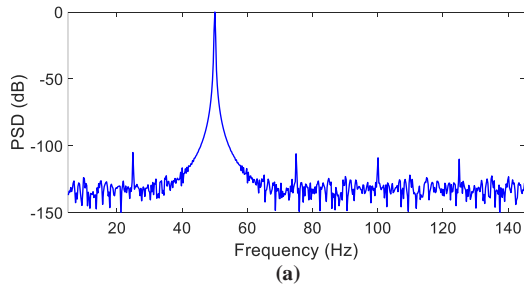


Fig. 12 Spectrum of the normalized line current (a) healthy motor (b) motor with 50%SE

Fig. 10 (a) shows  $F_y$  versus  $F_x$  in 50%SE. The force is in the direction of the minimum air gap, and its value is 545 and 570 N for the FEM and proposed model, respectively. In 50%DE, as shown in Fig. 10 (b), the force value is 475 and 500 N for the proposed model and FEM, respectively. Fig. 10 (c) demonstrates radial force components for the ME case with 40%SE and 30%DE. The force value is 550 and 570 N for the proposed model and FEM, respectively. It should be noticed that in high degrees of eccentricity (like 50%), saturation will be increased, and it affects the accuracy of the model. However, there is still a good agreement between the presented method and FEM. The peak value of the radial force on the rotor obtained from both the proposed method and FEM for different eccentricity types and degrees are summarized in Table II. It can be seen that the accuracy of the proposed model for the 20% SE and 20%DE is above 98%; also, the accuracy is above 95% in the case of 50%SE, 50%DE.

Fig. 11 illustrates the experimental results for the phasecurrent of the motor in different eccentricities. The current can be used for fault diagnosis purposes. Fig. 12 demonstrates

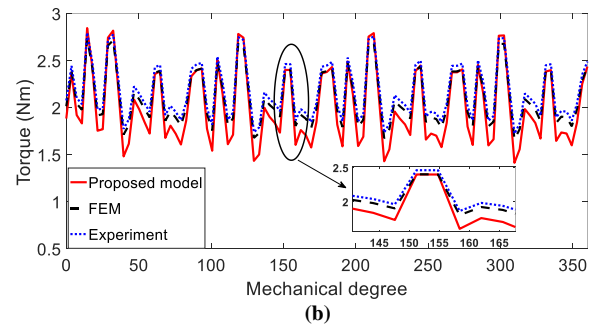
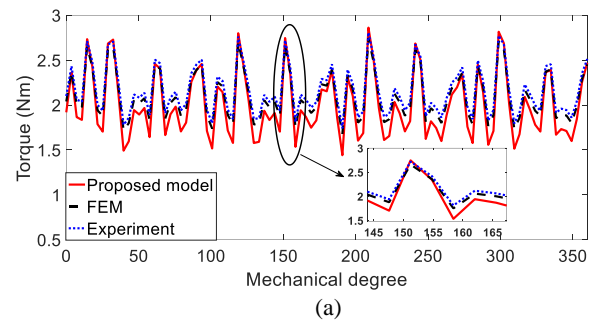


Fig. 13 Torque waveform comparison of the proposed model, FEM and experimental in (a) 50% SE (b) 50% DE

the normalized line current spectra of the SynRM for the healthy motor and motor with 50% SE, respectively. The amplitude of the sideband components around the main frequency (50Hz) is raised with the occurrence of the eccentricity. The specific frequency pattern, which is appeared in the motor current spectra can be used as an index for eccentricity fault diagnosis.

Fig.13 (a) and (b) show the comparison of the electromagnetic torque achieved from the proposed method, FEM, and experiments for the motor with 50%SE and 50% DE, respectively. As can be seen, the FEM and experimental test results, verify the accuracy of the proposed model.

## X. CONCLUSIONS

A numerical method based on the MWFM has been proposed to model different types of eccentricity in SynRMs. Using the proposed model, the motor inductances, air gap flux density, torque, and radial force on the rotor are calculated. The Maxwell Stress Tensor was used to predict electromagnetic torque. This model can be used for the preliminary design of SynRMs for EVs application. Moreover, it can be exploited for the dynamic simulation of SynRMs to obtain an appropriate index for use in the fault diagnosis systems such as MCSA. The comparison of the presented model with the FEM and experimental results have illustrated a good agreement. It should be pointed out that the computed radial force with the

proposed model is slightly higher than the FEM, especially at the severe eccentricities. However, this is useful in SynRMs design procedure to consider it as a safety factor. Besides, the time of simulation is a few seconds, while the FEM takes several hours. Therefore, the proposed method results are appropriate for the motor design purpose and fault diagnosis systems.

## REFERENCES

- [1] I. Boldea, L. N. Tutelea, L. Parsa, and D. Dorrell, "Automotive electric propulsion systems with reduced or no permanent magnets: An overview," *IEEE Transactions on Industrial Electronics*, vol. 61, no. 10, pp. 5696-5711, 2014.
- [2] G. V. Kumar, C.-H. Chuang, M.-Z. Lu, and C.-M. Liaw, "Development of an Electric Vehicle Synchronous Reluctance Motor Drive," *IEEE Transactions on Vehicular Technology*, vol. 69, no. 5, pp. 5012-5024, 2020
- [3] N. Bianchi, S. Bolognani, E. Carraro, M. Castiello, and E. Fornasiero, "Electric Vehicle Traction Based on Synchronous Reluctance Motors," *IEEE Transactions on Industry Applications*, vol. 52, no. 6, pp. 4762-4769, 2016/11 2016.
- [4] S. Taghavi and P. Pillay, "A sizing methodology of the synchronous reluctance motor for traction applications," *IEEE Journal of Emerging Selected Topics in Power Electronics*, vol. 2, no. 2, pp. 329-340, 2014.
- [5] A. Credo, G. Fabri, M. Villani, and M. Popescu, "Adopting the Topology Optimization in the Design of High-Speed Synchronous Reluctance Motors for Electric Vehicles," *IEEE Transactions on Industry Applications*, vol. 56, no. 5, pp. 5429-5438, 2020.
- [6] H. H. Safa, M. Ebrahimi, H. A. Zarchi, and M. Abshari, "Eccentricity fault detection in permanent magnet synchronous generators using stator voltage signature analysis," *International Journal of Precision Engineering and Manufacturing*, vol. 18, no. 12, pp. 1731-1737, 2017
- [7] M. S. Mirazimi and A. Kiyomarsi, "Magnetic Field Analysis of SynRel and PMASynRel Machines With Hyperbolic Flux Barriers Using Conformal Mapping," *IEEE Transactions on Transportation Electrification*, vol. 6, no. 1, pp. 52-61, 2020.
- [8] M. Farhadian, M. Moallem, and B. Fahimi, "Analytical calculation of magnetic field components in synchronous reluctance machine accounting for rotor flux barriers using combined conformal mapping and magnetic equivalent circuit methods," *Journal of Magnetism and Magnetic Materials*, p. 166762, 2020/03 2020.
- [9] S. S. Maroufian and P. Pillay, "Torque Characterization of a Synchronous Reluctance Machine Using an Analytical Model," *IEEE Transactions on Transportation Electrification*, vol. 4, no. 2, pp. 506-516, 2018.
- [10] S. G. Min and B. Sarlioglu, "Modeling and Investigation on Electromagnetic Noise in PM Motors With Single- and Double-Layer Concentrated Winding for EV and HEV Application," *IEEE Transactions on Transportation Electrification*, vol. 4, no. 1, pp. 292-302, March 2018
- [11] F. Rezaee-Alam, B. Rezaeealam, and J. Faiz, "Unbalanced Magnetic Force Analysis in Eccentric Surface Permanent-Magnet Motors Using an Improved Conformal Mapping Method," *IEEE Transactions on Energy Conversion*, vol. 32, no. 1, pp. 146-154, 2017.
- [12] D. G. Dorrell, "Calculation of unbalanced magnetic pull in small cage induction motors with skewed rotors and dynamic rotor eccentricity," *IEEE Transactions on Energy Conversion*, vol. 11, no. 3, pp. 483-488, 1996.
- [13] H. Kim, J. Nerg, T. Choudhury, and J. T. Sopenan, "Rotordynamic Simulation Method of Induction Motors Including the Effects of Unbalanced Magnetic Pull," *IEEE Access*, vol. 8, pp. 21631-21643, 2020.
- [14] M. Michon, R. C. Holehouse, K. Atallah, and G. Johnstone, "Effect of Rotor Eccentricity in Large Synchronous Machines," *IEEE Transactions on Magnetics*, vol. 50, no. 11, pp. 1-4, 2014.
- [15] J. J. Rocha Echeverria, P. V. V. da Silva, and E. da Costa Bortoni, "Analysis of Orbital Eccentricity and UMP in Large Salient Pole Synchronous Machines," *IEEE Transactions on Industry Applications*, vol. 55, no. 5, pp. 4715-4722, 2019.
- [16] Y. Zhou, X. Bao, C. Di and L. Wang, "Analysis of Dynamic Unbalanced Magnetic Pull in Induction Motor With Dynamic Eccentricity During Starting Period," *IEEE Transactions on Magnetics*, vol. 52, no. 7, pp. 1-4, July 2016.
- [17] D. G. Dorrell, "Sources and Characteristics of Unbalanced Magnetic Pull in Three-Phase Cage Induction Motors With Axial-Varying Rotor Eccentricity," *IEEE Transactions on Industry Applications*, vol. 47, no. 1, pp. 12-24, 2011.
- [18] A. Salah, Y. Guo and D. Dorrell, "Monitoring and damping unbalanced magnetic pull due to eccentricity fault in induction machines: A review," *2017 20th International Conference on Electrical Machines and Systems (ICEMS)*, Sydney, NSW, 2017, pp. 1-6.
- [19] D. G. Dorrell, J. K. H. Shek, M. A. Mueller and M. Hsieh, "Damper Windings in Induction Machines for Reduction of Unbalanced Magnetic Pull and Bearing Wear," *IEEE Transactions on Industry Applications*, vol. 49, no. 5, pp. 2206-2216, 2013.
- [20] H. H. Safa, M. Ebrahimi, A. Davoudi, and A. Pouramin, "Analytical Derivation of Induction Motors Inductances Under Eccentricity Conditions," *Progress In Electromagnetics Research B*, Vol. 60, 95-110, 2014.
- [21] C. Ma, H. Cui, P. Zheng, Y. Zhang and H. Gao, "Influence of static eccentricity on unbalanced magnetic force of external rotor permanent magnet brushless direct current motor used as In-wheel motor," *IET Electric Power Applications*, vol. 13, no. 4, pp. 538-550, 2019.
- [22] Y. Li, Q. Lu and Z. Zhu, "Unbalanced magnetic force prediction in permanent magnet machines with rotor eccentricity by improved superposition method," *IET Electric Power Applications*, vol. 11, no. 6, pp. 1095-1104, 2017.
- [23] C. Ma et al., "Effects of static eccentricity on the no-load back electromotive force of external rotor permanent magnet brushless DC motor used as in-wheel motor," *IET Electric Power Applications*, vol. 13, no. 5, pp. 604-613, 2019.
- [24] J. Ma and Z. Q. Zhu, "Mitigation of Unbalanced Magnetic Force in a PM Machine With Asymmetric Winding by Inserting Auxiliary Slots," *IEEE Transactions on Industry Applications*, vol. 54, no. 5, pp. 4133-4146, 2018.
- [25] J. Ren, X. Wang, W. Zhao and B. Peng, "Electromagnetic force density calculation in surface-mounted PM synchronous machine with rotor eccentricity by an equivalent transformation method," *IET Electric Power Applications*, vol. 14, no. 2, pp. 192-203, 2020.
- [26] H. Mahmoud and N. Bianchi, "Eccentricity in Synchronous Reluctance Motors—Part I: Analytical and Finite-Element Models," *IEEE Transactions on Energy Conversion*, vol. 30, no. 2, pp. 745-753, 2015.
- [27] G. Bacco, N. Bianchi, and H. Mahmoud, "A Nonlinear Analytical Model for the Rapid Prediction of the Torque of Synchronous Reluctance Machines," *IEEE Transactions on Energy Conversion*, vol. 33, no. 3, pp. 1539-1546, 2018.
- [28] H. Mahmoud and N. Bianchi, "Nonlinear Analytical Model of Eccentric Synchronous Reluctance Machines Considering the Iron Saturation and Slotting Effect," *IEEE Transactions on Industry Applications*, vol. 53, no. 3, pp. 2007-2015, 2017.
- [29] J. C. Moreira and T. A. Lipo, "Modeling of saturated AC machines including air gap flux harmonic components," *IEEE Transactions on Industry Applications*, vol. 28, no. 2, pp. 343-349, 1992.
- [30] J. Faiz and I. Tabatabaei, "Extension of winding function theory for nonuniform air gap in electric machinery," *IEEE Transactions on Magnetics*, vol. 38, no. 6, pp. 3654-3657, 2002/11 2002.
- [31] N. A. Al-Nuaim and H. Toliyat, "A novel method for modeling dynamic air-gap eccentricity in synchronous machines based on modified winding function theory," *IEEE Transactions on Energy Conversion*, vol. 13, no. 2, pp. 156-162, 1998.
- [32] K. J. Meessen, J. J. H. Paulides, and E. A. Lomonova, "Force Calculations in 3-D Cylindrical Structures Using Fourier Analysis and the Maxwell Stress Tensor," *IEEE Transactions on Magnetics*, vol. 49, no. 1, pp. 536-545, 2013.
- [33] Z. Wu and O. Ojo, "Coupled-circuit-model simulation and airgap-field calculation of a dual-stator-winding induction machine," *IEE Proceedings - Electric Power Applications*, vol. 153, no. 3, p. 387, 2006.
- [34] J. Faiz and M. Ojaghi, "Instantaneous-Power Harmonics as Indexes for Mixed Eccentricity Fault in Mains-Fed and Open/Closed-Loop Drive-Connected Squirrel-Cage Induction Motors," *IEEE Transactions on Industrial Electronics*, vol. 56, no. 11, pp. 4718-4726, 2009/11 2009.